




## Article

# Analysis and Design of Single-Phase Unidirectional Transducers with High Directivity

Xueping Sun <sup>1</sup>, Shaobo Ge <sup>1</sup>, Xiuting Shao <sup>2</sup>, Shun Zhou <sup>1</sup>, Wen Wang <sup>3</sup>, Dabin Lin <sup>1</sup> and Weiguo Liu <sup>1,\*</sup>

<sup>1</sup> School of Optoelectronic Engineering, Xi'an Technological University, Xi'an 710021, China; sunxueping.1988@163.com (X.S.); geshabo@126.com (S.G.); zsemail@126.com (S.Z.); dabinlin@xatu.edu.cn (D.L.)

<sup>2</sup> School of Information Science and Engineering, Shandong Normal University, Jinan 250358, China; shaoxiuting@126.com

<sup>3</sup> Institute of Acoustics, Chinese Academy of Sciences, Beijing 100190, China; wangwenwq@mail.ioa.ac.cn

\* Correspondence: wgliu@163.com

**Abstract:** Electrode-width-controlled (EWC) single-phase unidirectional transducers (SPUDT) contribute to reduction of insertion loss of surface acoustic wave (SAW) devices due to their strong unidirectional properties. In this work, we propose a method to optimize the unidirectionality of EWC-SPUDT based on our research results that the unidirectionality of the EWC-SPUDT cell is strongly related to its reflectivity and its unidirectional angle. Furthermore, in order to ensure strong unidirectionality to achieve low insertion loss, a simulator based on the finite element method (FEM) is used to study the relationship between geometrical configuration of the EWC-SPUDT cell and its reflection coefficient, as well as its transduction coefficient. Simulation results indicate that the reflection coefficient of the optimized EWC-SPUDT cell composed of 128° YX lithium niobite (LiNbO<sub>3</sub>) substrate and Al electrodes with thickness of 0.3μm reaches the optimal value of 5.17% when the unidirectional angle is designed to be −90°. A SAW delay line is developed with the optimized EWC-SPUDT cell without weighing, and the simulation results are verified by experiments. The experimental results show that the directivity exceeds 30 dB at the center frequency and the insertion loss is just 6.7 dB.

**Keywords:** single-phase unidirectional transducers (SPUDT); directivity; finite element method (FEM); Coupling-of-Modes (COM) theory



**Citation:** Sun, X.; Ge, S.; Shao, X.; Zhou, S.; Wang, W.; Lin, D.; Liu, W. Analysis and Design of Single-Phase Unidirectional Transducers with High Directivity. *Appl. Sci.* **2021**, *11*, 7500. <https://doi.org/10.3390/app11167500>

Academic Editor: Edoardo Piana

Received: 2 August 2021

Accepted: 13 August 2021

Published: 16 August 2021

**Publisher's Note:** MDPI stays neutral with regard to jurisdictional claims in published maps and institutional affiliations.



**Copyright:** © 2021 by the authors. Licensee MDPI, Basel, Switzerland. This article is an open access article distributed under the terms and conditions of the Creative Commons Attribution (CC BY) license (<https://creativecommons.org/licenses/by/4.0/>).

## 1. Introduction

Single-phase unidirectional transducers (SPUDT) are frequently employed in surface acoustic wave (SAW) devices to reduce bidirectional loss and to suppress triple transit echo [1–4]. Meanwhile, it is found that strengthening the unidirectionality is an effective way to suppress insertion loss. As is known, the SPUDT cells are the base elements of SPUDT. DART [5], electrode-width-controlled (EWC) [6], and other SPUDT cells [7,8] are the best-known cell types, of which the EWC-SPUDT is the most widely used. As shown in Figure 1, a traditional EWC-SPUDT cell consists of three fingers, two narrow electrodes, and one wide electrode, whose widths are  $\lambda/8$  and  $\lambda/4$ , respectively.  $\lambda$  is the electric period of the gratings. The distance between the two narrow finger is  $\lambda/8$ , and that between the narrow finger and the wide finger is  $3\lambda/16$ . In order to describe its performance, the following two parameters are listed: the reflectivity  $|\kappa|\lambda$ , and the unidirectional angle  $\theta$ , which is defined as  $\theta = \varphi_\kappa - 2\varphi_\alpha$ , where  $\varphi_\kappa$  and  $\varphi_\alpha$  are the phases of reflection coefficient and transduction, respectively [9]. According to our calculation of a traditional EWC-SPUDT cell,  $|\kappa|\lambda$  is 1.37% and  $\theta$  is  $-83.58^\circ$ , which are very close to the results presented in [10].

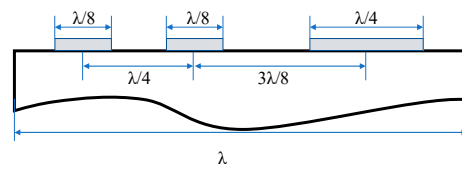


**Figure 1.** The geometrical configuration of an EWC-SPUDT cell.

Hashimoto et al. utilized finite element method (FEM) and spectral domain analysis (SDA) to analyze the SAW propagation characteristics under a type of triple electrodes grating (an improved EWC-SPUDT), but they failed to find how the geometric structure influences its unidirectionality and how to optimize its structure [11]. Yongan Shui et al. studied the optimal design of the three fingers, including their position and width, using the periodical Green's function method, but they did not explicate the influence of these parameters on the reflectivity and unidirectional angle [10]. Sho Nakagomi and Honglang Li chose Cu electrodes instead of Al electrodes to achieve greater mechanical reflection [12,13] since the density of Cu is greater than that of Al; however, they neglected the fact that the electrical and mechanical reflection caused by short-circuited gratings consisting of either Cu or Al on  $128^\circ$  YX-LiNbO<sub>3</sub> substrate are opposite and cancel each other.

The purpose of this paper is to enhance the unidirectionality of the EWC-SPUDT and further reduce its insertion loss by improving the reflection characteristics of the transducer as much as possible, based on the premise that the minimum width of the electrodes is limited and the unidirectional angle is  $-90^\circ$ . In addition, the design principles of EWC-SPUDT are discussed theoretically and experimentally.

## 2. Design and Optimization

The basic idea of an EWC-SPUDT is to place a distributed reflection source in a normal interdigital SAW transducer to enhance the forward acoustic wave and meanwhile reduce that traveling along the backward direction [6]. Scattering matrix is an effective description of the performance of the SAW transducers with well impedance matching, especially when designing filters. The expressions of scattering matrix parameters  $S_{11}$  and  $S_{13}$  are given below.

$$S_{11} = P_{11} + \frac{2P_{13}^2}{G_L + P_{33}} \quad (1)$$

$$S_{13} = \frac{2\sqrt{G_L}P_{13}}{G_L + P_{33}} \quad (2)$$

In Equations (1) and (2),  $P_{11}$ ,  $P_{13}$ , and  $P_{33}$  are the elements of P-matrix. In an interdigital transducer,  $P_{11}$  is the reflection coefficient,  $P_{13}$  describes the excitation efficient, and  $P_{33}$  denotes the transducer admittance, which describes the acoustic and electrostatic currents due to a drive voltage. Their detailed expressions are given in [14–16].  $G_L$  is the combined effective electrical load conductance which is attached to the SPUDT electrical port. The goal for designing a SPUDT filter is to make a zero  $S_{11}$  under matched conditions and provide a desired magnitude and phase response for  $S_{13}$ . From Equation (1),  $G_L$  is required to match the SPUDT if found by equating  $S_{11}$  to zero [17].

$$G_L = -P_{33} - \frac{2P_{13}^2}{P_{11}} \quad (3)$$

If a lossless SPUDT is tuned using a lossless matching network, its insertion loss under the condition of optimum matching will be related to the following parameters: the unidirectional angle  $\theta$ , the product of the reflectivity per unit length, and the effective reflection length  $|\kappa|L$ . After substituting P-matrix elements into (2), the insertion loss can

be obtained. The minimum insertion loss of the SPUDT occurs when  $\theta$  equals  $-90^\circ$ , and then its expression evolves into the following form:

$$|S_{13}|^2 = 1 - \exp(-2|\kappa|L) \quad (4)$$

A similar result was presented in [17].

Equation (4) implies that the insertion loss can be reduced by increasing the reflectivity of the SPUDT. The directivity  $D$ , defined as the ratio between the two acoustic outputs for an interdigital transducer (IDT), is given by  $D = |P_{32}/P_{31}|$ . It can be simplified to (5) at center frequency.

$$D = \left| \frac{1 + j \exp(j\theta) \tanh(|\kappa|L/2)}{1 + j \exp(-j\theta) \tanh(|\kappa|L/2)} \right| \quad (5)$$

where  $j$  is an imaginary unit.

When  $D > 1$ , the wave excitation in the right direction is greater than that in the left direction, while when  $D < 1$ , the situation is just the opposite. In addition,  $D = 1$  means that the transducer is bidirectional. It can be clearly seen from the expression above that  $D$  tends to increase with the increase in  $|\kappa|L$ , and when  $\theta = -90^\circ$ ,  $D$  reaches the maximum value  $\exp(|\kappa|L)$ .

In summary, optimizing the EWC-SPDUT cell is to maximize its reflectivity at a unidirectional angle of  $-90^\circ$ . Next, we will discuss the relationship between the geometry of the EWC-SPUDT cell and its unidirectional angle, as well as its reflectivity combining the coupling-of-modes (COM) theory. The governing equations of COM can be written as [14,18,19]:

$$\begin{cases} \frac{\partial R(x)}{\partial x} = -i\delta R(x) + i\kappa S(x) + i\alpha V \\ \frac{\partial S(x)}{\partial x} = -i\kappa^* R(x) + i\delta S(x) - i\alpha^* V \\ \frac{\partial i}{\partial x} = -2i\alpha^* R(x) - 2i\alpha S(x) + i\omega CV \end{cases} \quad (6)$$

where  $R(x)$  and  $S(x)$  are the amplitudes of the waves propagating in positive and negative  $x$ , respectively.  $i$  is the current on the busbar and  $V$  is the applied voltage.  $\omega$  is the angular frequency.  $\delta = \frac{\omega}{v} - \frac{2\pi}{\lambda}$  is a detuning parameter. The four independent parameters of the model are the effective SAW velocity  $v$ , the reflection coefficient per unit length  $\kappa$ , the transduction coefficient per unit length  $\alpha$ , and the static capacitance per unit length  $C$ .

The four COM parameters can be calculated by FEM [20,21]. This approach allows accurate calculation of the transduction amplitude, reflectivity, and the unidirectional angle for any cell geometry. There are five parameters, including the widths of the three fingers and the distances between adjacent fingers, which need to be determined in the EWC-SPUDT cell. It would be a huge undertaking to optimize all of these five parameters at the same time, and the physical meaning of the geometry would be unclear. Therefore, it is necessary to understand the influence of each finger on reflectivity and other COM parameters.

In this paper, calculations were conducted by FEM with the commercial software package COMSOL Multiphysics. Al was selected as the electrode material and  $128^\circ$  YX LiNbO<sub>3</sub> was chosen as the substrate due to its high coupling coefficients ( $K^2 \cong 5.6\%$ ) [22]. Our previous studies demonstrated that the reflectivity is strongly dependent on the normalized electrode thickness  $h/\lambda$ , which first increases and then decreases with an increase in electrode thickness [23]. Accordingly, a thin Al electrode with  $h/\lambda = 0.6\%$  is chosen to provide adequate reflectivity.

Compared with widely used FEM/BEM hybrid methods [24,25], FEM has obvious advantages, especially its remarkable generality. It can be used to analyze a SPUDT composed of arbitrary materials, crystal cuts, as well as different electrode shapes [26–31]. Therefore, we use FEM to calculate the parameters needed for simulation and then to optimize the design of the transducer structure. Firstly, the structural model of the transducer unit is established as shown in Figure 2, and the influence of the electrode width on the reflectivity is discussed by taking the electrode width as a variable.

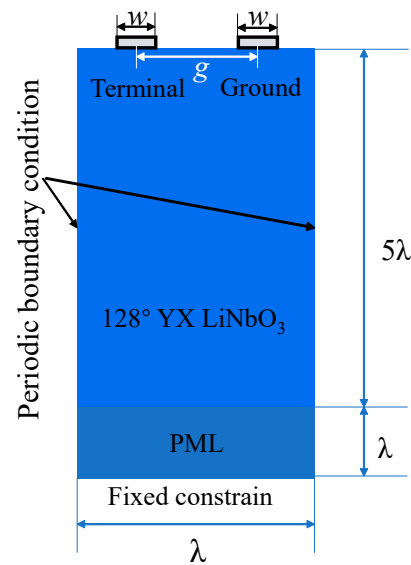


Figure 2. FEM model of an IDT unit cell with boundary conditions.

To suppress reflections of SAW from the bottom, an additional 128° YX LiNbO<sub>3</sub> layer of 1λ is attached at the bottom as a perfect matching layer (PML) [32,33]. The top surface is mechanically free, while the bottom is fixed. Mechanical and electrical periodic conditions are applied on both sides of the unit model [34,35]. The left electrode is assigned as the electrical terminal with  $V = 1$ , while the right one is grounded.

The reflectivity can be calculated by Equation (7):

$$|\kappa|\lambda = 2\pi \frac{f_{s+} - f_{s-}}{f_{s+} + f_{s-}} \tag{7}$$

where  $f_{s+}$  and  $f_{s-}$  stand for the anti-symmetric and symmetric frequencies, respectively. The relationships between the reflectivity and the width of two fingers  $w$  and their distance  $g$  are depicted in Figure 3, from which two conclusions can be drawn: (i) The reflectivity reaches its maximum value when  $g$  approaches and this is because the phase difference between the SAW reflected by the second finger and that reflected by the first finger is  $2\pi$ , resulting in in-phase superposition; (ii) When  $g = \lambda/2$ , the reflectivity increases at first and then decreases with the increase in electrode width, and the maximum value of 5.56% occurs at about  $w = 3\lambda/32$ . A measured electrode reflectivity given in [36] confirms our conclusion.

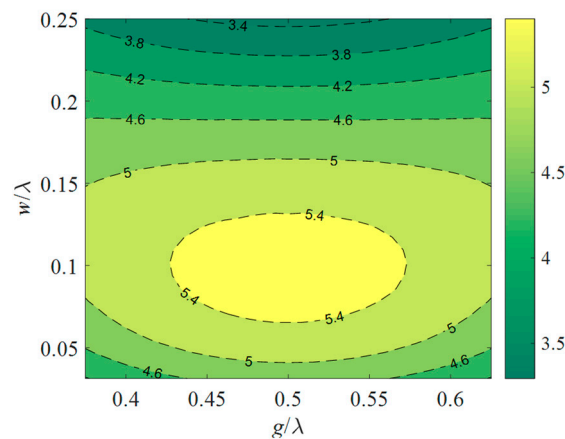


Figure 3. Reflectivity per period of Al electrodes on 128° YX LiNbO<sub>3</sub> substrate.

As shown in Figure 1, the EWC-SPUDT cell consists of three fingers. The first finger plays the role of generating surface acoustic waves; however, it also reflects the incident acoustic waves, while the reflection can be cancelled out with the entry of the second finger. The function of the third finger is mainly to enhance the reflection, and its position deviation from the transduction center of  $\lambda/8$  is so that the acoustic wave can produce constructive interference in the forward propagation direction while producing destructive interference in the backward propagation direction. Therefore, we reduce the width of the first electrode to the minimum width limited by the process conditions (in this paper  $2\mu\text{m}$  is the minimum width) and set the width of the remaining two fingers to  $3\lambda/32$ . Finally, the spacing of the fingers is adjusted according to the results of the FEM simulation. The optimization model of EWC-SPUDT periodic structure is established as shown in Figure 4.

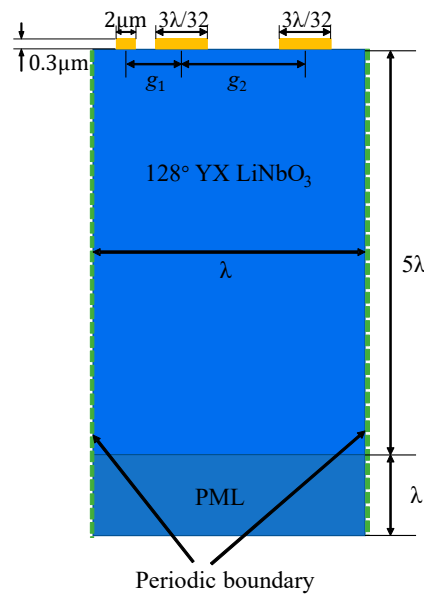


Figure 4. Optimized model of an EWC-SPUDT structure unit.

In the analysis, the thickness of the electrodes and the wavelength of SAW were set at two fixed values of  $0.3\ \mu\text{m}$  and  $50\ \mu\text{m}$ , respectively. Except for the electrical boundary conditions, other boundary conditions are consistent with Figure 2. In the COM analysis, cosine of  $\theta$  can be expressed as the following formula [37,38]:

$$\cos(\theta) = \frac{(f_{o+} - f_{o-})^2 - (f_{s+} - f_{s-})^2 - ((f_{o+} + f_{o-}) - (f_{s+} + f_{s-}))^2}{2(f_{s+} - f_{s-})((f_{o+} + f_{o-}) - (f_{s+} + f_{s-}))} \quad (8)$$

where  $f_{o+}$  and  $f_{o-}$  are the upper edge and lower edge frequencies of the stopband responding to the anti-symmetry and symmetry frequencies in open-circuited grating eigenmodes, while  $f_{s+}$  and  $f_{s-}$  are the upper edge and lower edge frequencies of the stopband responding to the anti-symmetry and symmetry frequencies in short-circuited grating eigenmodes, respectively.

However, using Equation (8), it is difficult to determine the sign of  $\theta$ . Therefore, the displacements at lower frequencies in short-circuited and open-circuited gratings are resorted to for the calculation of  $\theta$ , the method of which is presented in another article to be published. Equation (8) can be used to check the accuracy of  $\theta$ . In a short-circuited grating, the first finger is assigned as the electrical terminal with  $V = 1$  and the other two fingers are assigned as the electrical terminal with  $V = 0$ . While in an open-circuited grating, all three fingers are assigned as the electrical terminal with charge  $Q = 0$ . We set the two gaps as:  $g_1$ , ranging from  $0.1069\lambda$  to  $0.15\lambda$ , and  $g_2$ , ranging from  $11\lambda/32$  to  $15\lambda/32$ . Then, the reflectivity and the unidirectional angle can be calculated. In Figure 5, we show the reflectivity contour map and a contour map of  $\theta = -90^\circ$  is also shown. This way it

is easy to find the optimization conditions mentioned before: increasing  $|\kappa|\lambda$  as soon as possible with constraint condition  $\theta = -90^\circ$  being met. The  $\varphi_\kappa$  and  $\varphi_\alpha$ , which determine the unidirectional angle, are also expressed in contour maps (see Appendix A, Figure A3). In Appendix A, we show graphs of all the COM parameters of EWC-SPUDT with different  $g_1$  and  $g_2$  values.

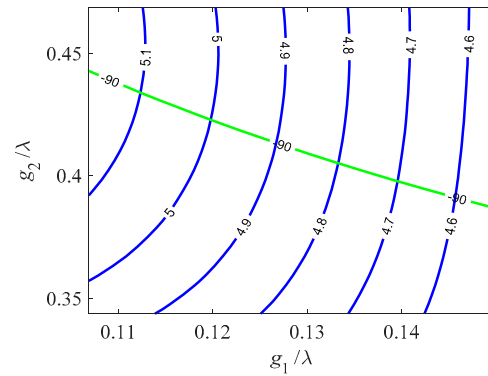


**Figure 5.** Reflectivity and unidirectional angle dependence on the two gaps between three fingers.

### 3. Fabrication Technologies

As shown in Figure 5, on the premise of limiting the width of the three electrode fingers to  $2\mu\text{m}$ ,  $3/32\lambda$ , and  $3/32\lambda$ , the reflection coefficient and unidirectional angle reach their optimal values  $|\kappa|\lambda = 5.17\%$  and  $\theta = -90^\circ$ , respectively, when the finger spaces are  $g_1 = 0.1069\lambda$  and  $g_2 = 0.4414\lambda$ . Due to EWC-SPUDT being a kind of unidirectional transducer—which means that the characteristics of the SAW propagation along the forward and backward directions are different—it is necessary to study the frequency responses of acoustic waves in two directions.

According to our analysis based on the COM theory, the transducers face-to-face, corresponding to the forward direction, shown in Figure 6a have a lower insertion loss near the center frequency than that of the transducers back-to-back, corresponding to the backward direction, as shown in Figure 6b. To verify the conclusion above, transducers both face-to-face and back-to-back, based on optimized EWC-SPUDT cells, were developed and performance experiments were carried out.

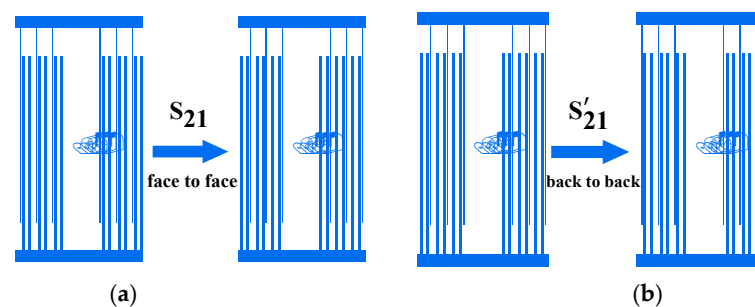


**Figure 6.** Test device configuration with (a) transducers face-to-face and (b) transducers back-to-back.

Figure 7 shows the processing procedure for developing SAW devices. In our experiments, the AZ5214 reversal photoresist was used for ultraviolet (UV) photolithography. After lithography, Al film of 300 nm thickness was deposited on  $128^\circ$  YX LiNbO<sub>3</sub> substrate by magnetron sputtering. Then, the conventional lift-off technique was utilized to remove the regions of photoresist [39,40]. Each SAW delay line consists of input interdigital IDTs and output IDTs, each of them including 73 pairs of EWC-SPUDT cells with an aperture of  $50\lambda$ . Figure 8 presents an optical microscope image of the SAW device fabricated by the conventional lift-off technique. Specifically, as mentioned above, transducers face-to-



face and back-to-back based on traditional EWC-SPUDT cells were also developed for comparative experiments.

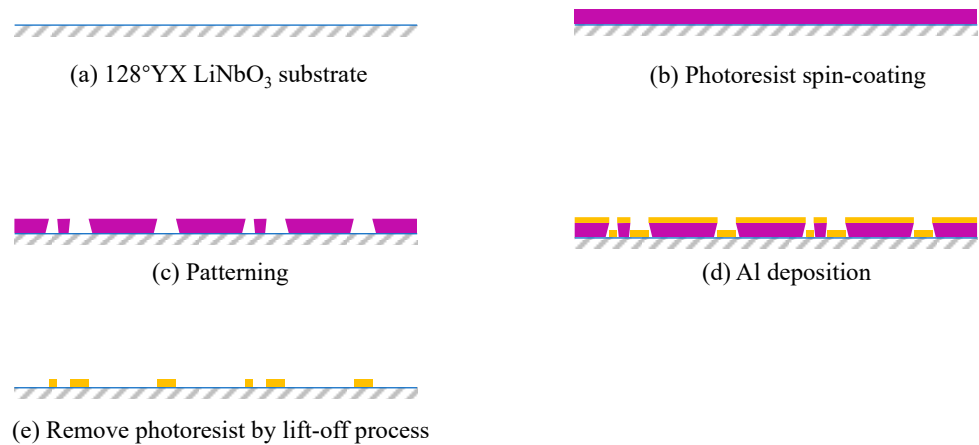


**Figure 7.** Fabrication procedure for a test device.

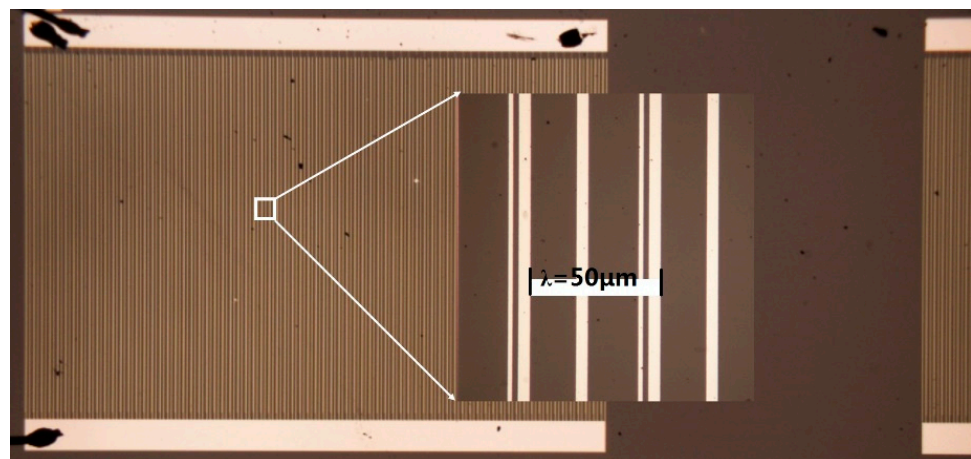
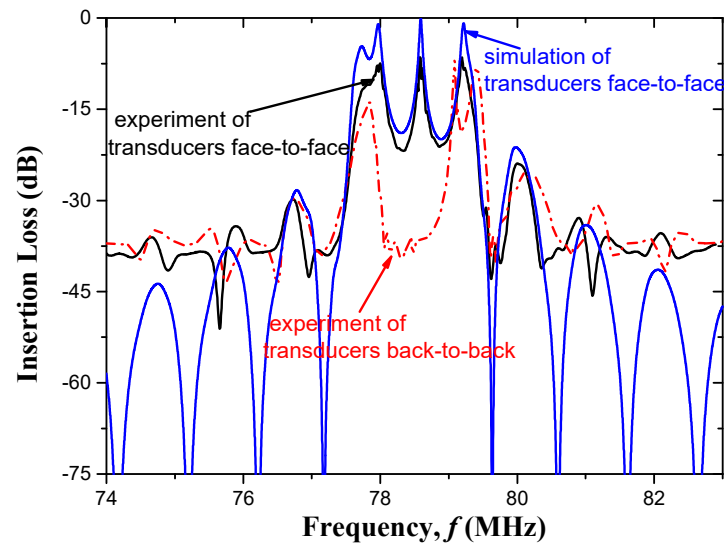


**Figure 8.** Image of the fabricated test device with transducers face-to-face.

#### 4. Experimental Results and Discussion

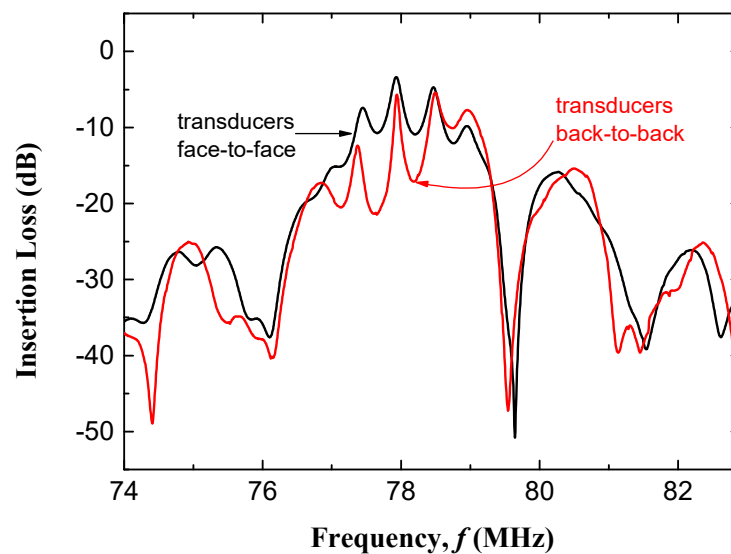
The other COM parameters can also be obtained by the FEM method; then, the P-matrix for each EWC-SPUDT cell, which is a very effective tool for analyzing and designing SAW devices, can be constructed [41–43]. The overall response of the whole device can be determined by the cascading of the P-matrixes of each individual part of the device. In this way, we can easily calculate the transmission scattering parameters ( $S_{21}$ ) of a SAW delay line and further calculate its insertion loss (by the equation  $IL = -20 \log_{10}(S_{21})$ ) through combining the input IDTs and the output IDTs with electrical source or load. Therefore, the theoretical value of electrode insertion loss can be calculated by COM theory, while the experimental value can be obtained by network analyzer (Agilent E5061B).

Figure 9 shows the calculated and experimental results of transducers with the optimized EWC-SPUDT cells. These results include the calculated and experimental responses with the transducers face-to-face, and the experimental response of the transducers back-to-back as a contrast. The results indicate that the simulation results coincide with the experimental results expected at the side-lobes, that is to say, the experiment confirms that our theoretical analysis process is reasonable. It is easy to see that the response of the transducers based on two structures is indeed different near the center frequency, and that the transducers face-to-face have better performance than the other one.



**Figure 9.** Frequency responses of the test devices with optimized EWC-SPUDT cells.

In addition, as a contrast, two SAW delay lines with traditional EWC-SPUDT cells were designed, fabricated, and measured. The insertion loss of the transducers face-to-face ( $IL = -20 \log_{10}(S_{21})$ ) and back-to-back ( $IL = -20 \log_{10}(S'_{21})$ ) are shown in Figure 10. The results show that the response near the center frequency with transducers face-to-face is better than with the transducers back-to-back, but the difference is not obvious.



**Figure 10.** Frequency responses of the test devices with traditional EWC-SPUDT cells.

The elements of  $P$ -matrix are related to the scattering coefficient, therefore, the directivity  $D$  in logarithmic form can also be approximately expressed as  $-20 \log_{10}(S_{21}/S'_{21})$ . The frequency dependence of  $D$  for an optimized EWC-SPUDT compared with that for a traditional EWC-SPUDT is shown in Figure 11. The maximum directivity of transducer based on the optimized EWC-SPUDT cells reaches 30.1 dB, which is much larger than that based on the traditional EWC-SPUDT cell. It suggests that the optimized EWC-SPUDT cell can be used to achieve miniaturization and higher performance in SAW device design.



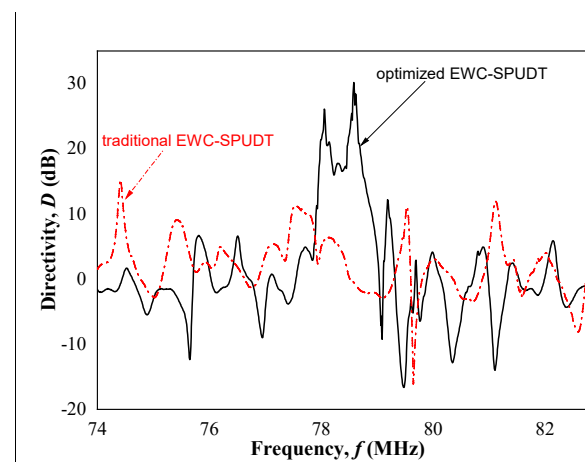


**Figure 11.** Comparison on the directivity of test devices with optimized EWC-SPUDT cells and with traditional EWC-SPUDT cells.

## 5. Conclusions

The structural optimization of an EWC-SPUDT cell was discussed. The influence of the geometry of an EWC-SPUDT cell on its reflectivity and its unidirectional angle were investigated by FEM, and the optimized structure parameters under some certain restrictions were obtained. Several SAW devices based on the optimized EWC-SPUDT cells and traditional EWC-SPUDT cells were designed and fabricated to verify our theoretical analysis results. The experimental results show that the minimum insertion loss of the SAW device based on the optimized cells is as low as 6.7 dB, and the directivity is as high as 30.1 dB, which are much better than those based on traditional EWC-SPUDT cells. All of the results demonstrate that the optimized EWC-SPUDT cell could further be used to enhance the performance of SAW devices. Although the narrow electrode width limits its application in the high frequency field, the method proposed in this paper can also be used to improve performance, to some extent, when the finger width is set to a certain value.

**Author Contributions:** Conceptualization, W.L. and W.W.; methodology, software, and writing, X.S. (Xueping Sun); investigation and validation, X.S. (Xiuting Shao) and S.G.; formal analysis, D.L.; resources and data curation, S.Z.; funding acquisition, W.L. and X.S. (Xiuting Shao). All authors have read and agreed to the published version of the manuscript.

**Funding:** The authors would like to acknowledge support from the Advanced Optical Manufacturing and Detection Innovation Team project of Shaanxi Provincial Science and Technology Department, grant number 2017KCT-08-02. The work presented in this paper was also supported by the Key Laboratory for Equipment Pre-research under grant number 6142207190407 and the National Natural Science Foundation of China under grant number 11804201.

**Institutional Review Board Statement:** Not applicable.

**Informed Consent Statement:** Not applicable.

**Data Availability Statement:** Not applicable.

**Conflicts of Interest:** The authors declare no conflict of interest.

## Appendix A

In the equations of COM model, the COM parameters are the effective SAW velocity  $v$ , the reflection coefficient per unit length  $\kappa$ , the transduction coefficient per unit length  $\alpha$ , and the static capacitance per unit length  $C$ . There are six parameters in a structure due to a complex reflection coefficient and a complex transduction coefficient. In the following materials, we present all of the COM parameters in graphs to show their variations of different finger spaces  $g_1$  and  $g_2$ .

The effective SAW velocity under short-circuited grating is shown in Figure A1.

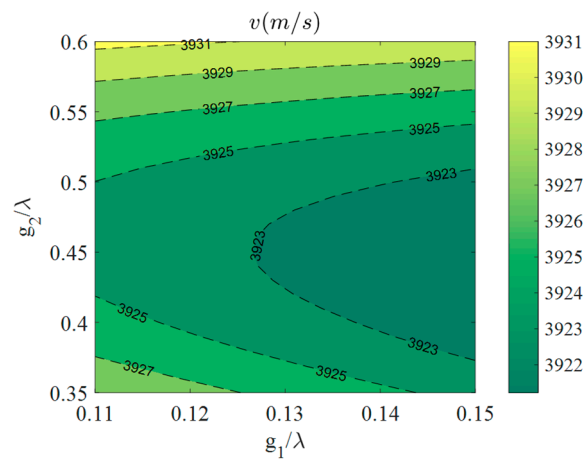


Figure A1. Contour of  $v$  as a function of  $g_1$  and  $g_2$ .

The magnitude of the normalized reflectivity with an electrical period  $\lambda$  is shown in Figure A2.

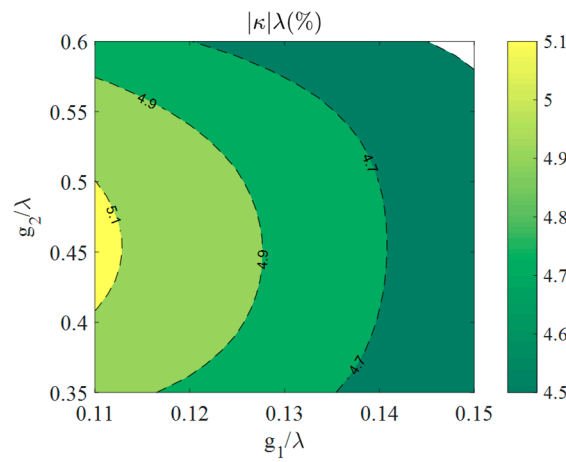


Figure A2. Contour of  $|\kappa\lambda|$  as a function of  $g_1$  and  $g_2$ .

$\varphi_k$  and  $\varphi_\alpha$  are shown in Figure A3a,b, respectively.

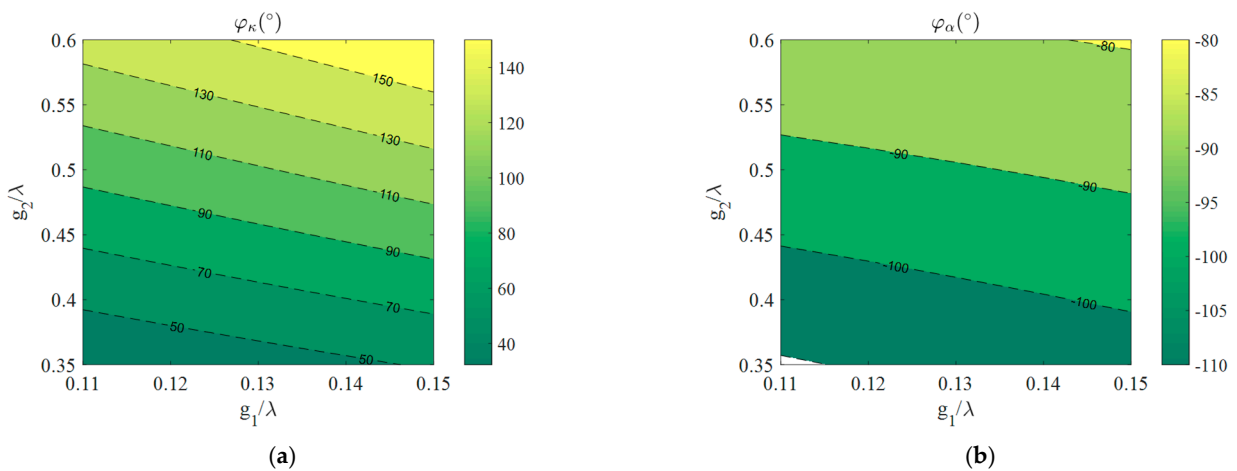
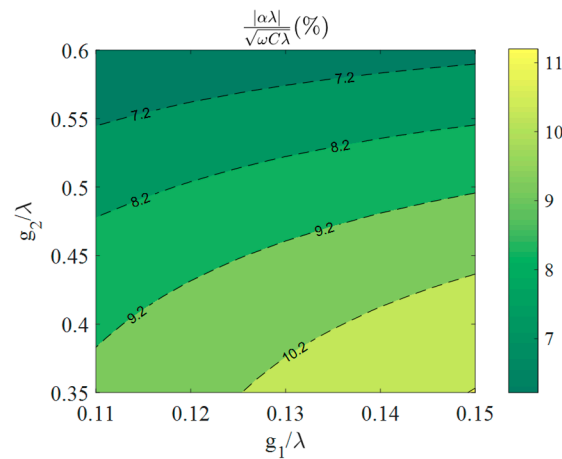


Figure A3. (a) Contours of  $\varphi_k$  and (b)  $\varphi_\alpha$  as a function of  $g_1$  and  $g_2$ .

We normalized the transduction coefficient as  $\frac{|\alpha\lambda|}{\sqrt{\omega C\lambda}}$ , shown in Figure A4.



**Figure A4.** Contour of the transduction coefficient as a function of  $g_1$  and  $g_2$ .

We processed the unidirectional angle  $\theta$  with  $\theta = \theta - 360$  so that it is in the range of  $-180^\circ$  to  $180^\circ$ , shown in Figure A5.

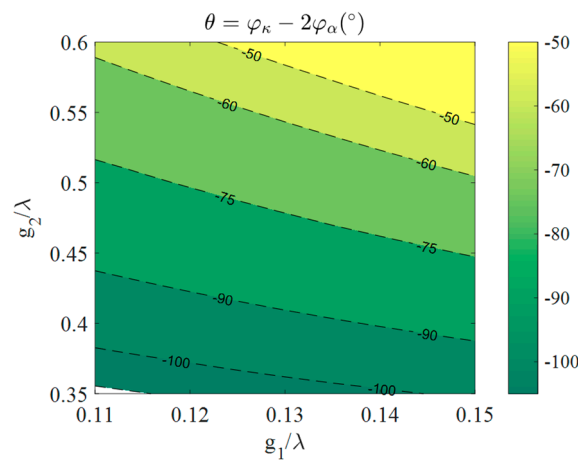


**Figure A5.** Contour of  $\theta$  as a function of  $g_1$  and  $g_2$ .

The normalized capacitance  $C\lambda$  means capacitance per electrical period and per unit length of aperture, shown in Figure A6.

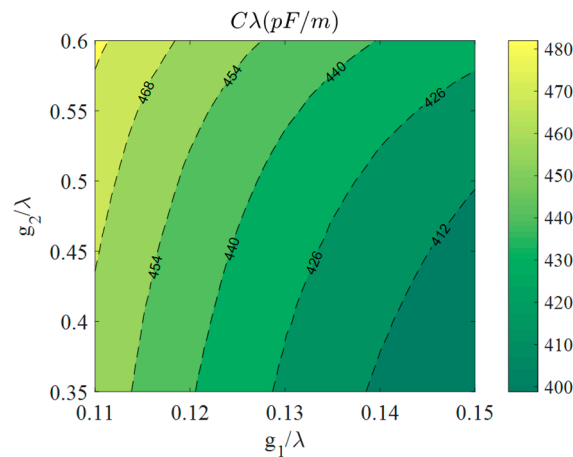


**Figure A6.** Contour of normalized capacitance as a function of  $g_1$  and  $g_2$ .

## References

1. Wang, W.; Shao, X.; Liu, X.; Liu, J.; He, S. Enhanced sensitivity of Surface acoustic wave-based rate sensors incorporating metallic dot arrays. *Sensors* **2014**, *14*, 3908–3920.
2. Lu, R.; Manzaneque, T.; Yang, Y.; Li, M.H.; Gong, S. Gigahertz low-loss and wideband S0 mode lithium niobate acoustic delay lines. *IEEE Trans. Ultrason. Ferroelectr. Fre. Control* **2019**, *66*, 1373–1386. [[CrossRef](#)]
3. Chung, M.H.; Hwang, R.C.; Chiu, J.J.; Yang, M.W.; Hung, T.T.; Shen, C.Y. Enhanced sensitive surface acoustic wave device designed for nitric oxide gas detection. *Sensor Mater.* **2019**, *31*, 2195–2212. [[CrossRef](#)]
4. Manzaneque, T.; Lu, R.; Yang, Y.; Gong, S. Low-loss and wideband acoustic delay lines. *IEEE Trans. Microw. Theory Tech.* **2019**, *67*, 1379–1391. [[CrossRef](#)]
5. Kodama, T.; Kawabata, H.; Sato, H.; Yasuhara, Y. Design of low-loss SAW filters employing distributed acoustic reflection transducers. In Proceedings of the IEEE Ultrasonics Symposium, Williamsburg, VA, USA, 17–19 November 1986; pp. 59–64. [[CrossRef](#)]
6. Hartmann, C.S.; Abbott, B.P. Overview of design challenges for single phase unidirectional SAW filters. In Proceedings of the IEEE Ultrasonics Symposium, Montreal, QC, Canada, 3–6 October 1989; pp. 79–89. [[CrossRef](#)]
7. Yamanouchi, K.; Furuyashiki, H. Low-loss SAW filter using internal reflection types of new single-phase unidirectional transducer. In Proceedings of the IEEE Ultrasonics Symposium, Dallas, TX, USA, 14–16 November 1984; pp. 68–71. [[CrossRef](#)]
8. Chvets, V.B.; Ivanov, P.G.; Makarov, V.M.; Orlov, V.S. Low-loss SAW filters using new SPUDT structures. In Proceedings of the IEEE Ultrasonics Symposium, Toronto, ON, Canada, 5–8 October 1997; pp. 69–72. [[CrossRef](#)]
9. Galipeau, J.D. Enhanced SPUDT cells for high coupling substrates. In Proceedings of the IEEE Ultrasonics Symposium, Rotterdam, The Netherlands, 18–21 September 2005; pp. 1052–1055. [[CrossRef](#)]
10. Shui, Y.; Lin, J.M.; Wu, H.; Wang, N.; Chen, H. Optimization of single-phase, unidirectional transducers using three fingers per period. *IEEE Trans. Ultrason. Ferroelectr. Fre. Control* **2002**, *49*, 1617–1621. [[CrossRef](#)]
11. Hashimoto, K.Y.; Zheng, G.Q.; Yamaguchi, M. Fast analysis of SAW propagation under multi-electrode-type gratings with finite thickness. In Proceedings of the IEEE Ultrasonics Symposium, Toronto, ON, Canada, 5–8 October 1997; pp. 279–284. [[CrossRef](#)]
12. Li, H.; Wen, J.; Hashimoto, K.Y.; Omori, T.; Yamaguchi, M. Low-loss and constant-group-delay surface acoustic wave filters employing Cu-based resonant single-phase unidirectional transducers. *Jpn. J. Appl. Phys.* **2006**, *45*, 4655–4657. [[CrossRef](#)]
13. Nakagomi, S.; Asano, H.; Tanaka, H.; Omori, T.; Hashimoto, K.Y.; Yamaguchi, M. Single-phase unidirectional surface acoustic wave transducer using Cu electrode. *Jpn. J. Appl. Phys.* **2003**, *42*, 3152–3156. [[CrossRef](#)]
14. Plessky, V.; Koskela, J. Coupling-of-modes analysis of SAW devices. *Int. J. High Speed Electron. Syst.* **2000**, *10*, 867–947. [[CrossRef](#)]
15. Tian, Y.; Li, H.; Ke, Y.; Yuan, C.; He, S. P-Matrix Analysis of Surface Acoustic Waves in Piezoelectric Phononic Crystals. *IEEE Trans. Ultrason. Ferroelectr. Fre. Control* **2016**, *63*, 757–763. [[CrossRef](#)]
16. Mayer, M.; Dadgar-Javid, G.; Ebner, T.; Wagner, K. Causal P-matrix description of leaky SAW devices. In Proceedings of the IEEE Ultrasonics Symposium, Tours, France, 18–21 September 2016; pp. 1–4. [[CrossRef](#)]
17. Abbott, B.P.; Hartmann, C.S.; Malocha, D.C. Matching of single-phase unidirectional SAW transducers and a demonstration using a low-loss EWC/SPUDT filter. In Proceedings of the IEEE Ultrasonics Symposium, Honolulu, HI, USA, 4–7 December 1990; pp. 49–54. [[CrossRef](#)]
18. Lin, J.; Wang, N.; Chen, H.; Shui, Y. Fast, precise, and full extraction of the COM parameters for multielectrode-type gratings by periodic Green's function method. *IEEE Trans. Ultrason. Ferroelectr. Fre. Control* **2002**, *49*, 1735–1738. [[CrossRef](#)]
19. Chen, D.P.; Haus, H.A. Analysis of metal-strip SAW gratings and transducers. *IEEE Trans. Sonics Ultrason* **1985**, *32*, 395–408. [[CrossRef](#)]
20. Sun, X.; Liu, W.; Ge, S.; Zhou, S.; Li, X.; Lin, D. Achieving both high electromechanical response and stable temperature behavior in Si/SiO<sub>2</sub>/Al/LiTaO<sub>3</sub> sandwich structure. *AIP Adv.* **2019**, *9*, 35145. [[CrossRef](#)]
21. Zhang, Y.M.; Jin, J.; Li, H.L.; Hu, H.P. A novel method to extract COM parameters for SAW based on FEM. In Proceedings of the 2019 13th Symposium on Piezoelectricity, Acoustic Waves and Device Applications (SPAWDA), Harbin, China, 11–14 January 2019; pp. 1–5. [[CrossRef](#)]
22. Carmichael, C.; Malocha, D.C.; Weeks, A. Asymmetric energy coupling through acoustoelectric effect using graphene on lithium niobate surface acoustic wave delay line in GHz Range. In Proceedings of the IEEE Ultrasonics Symposium, Glasgow, UK, 6–9 October 2019; pp. 702–705. [[CrossRef](#)]
23. Sun, X.; Liu, W.; Shao, X.; Zhou, S.; Wang, W.; Lin, D. Surface acoustic wave gyroscopic effect in an interdigital transducer. *Sensors* **2018**, *19*, 106. [[CrossRef](#)] [[PubMed](#)]
24. Solal, M.; Chen, L.; Gratier, J. Measurement and FEM/BEM simulation of transverse effects in SAW resonators on lithium tantalite. *IEEE Trans. Ultrason. Ferroelectr. Fre. Control* **2013**, *60*, 2404–2413. [[CrossRef](#)]
25. Dufilie, P.; Ventura, P.; Hecht, F. COM parameters for thick metal and partially buried electrodes extracted from a mixed FEM/BEM numerical model. In Proceedings of the IEEE Ultrasonics Symposium, Dresden, Germany, 7–10 October 2012; pp. 807–810. [[CrossRef](#)]
26. Matsuoka, N.; Li, X.; Omori, T.; Hashimoto, K.Y. Study of loss mechanisms in temperature compensated surface acoustic wave devices based on finite element method analysis using hierarchical cascading technique. *Jpn. J. Appl. Phys.* **2020**, *59*, SKKC06. [[CrossRef](#)]

27. Wang, T.; Green, R.; Guldiken, R.; Wang, J.; Mohapatra, S.; Mohapatra, S.S. Finite element analysis for surface acoustic wave device characteristic properties and sensitivity. *Sensors* **2019**, *19*, 1749. [[CrossRef](#)]
28. Xiao, Q.; Dai, M.; Chen, J.; Fan, Y.P.; Cai, P.; Ji, X.J. Surface acoustic wave characteristics with a layered structure of IDT/ $\theta^\circ$  YX-LiTaO<sub>3</sub>/SiO<sub>2</sub>/AlN /diamond. *Acoust. Phys.* **2020**, *65*, 652–657. [[CrossRef](#)]
29. Koskela, J.; Plessky, V. Hierarchical Cascading in FEM Simulations of SAW Devices. In Proceedings of the IEEE Ultrasonics Symposium, Kobe, Japan, 22–25 October 2018; pp. 1–11. [[CrossRef](#)]
30. Xie, Q.; Hu, Y.; Zhao, X.; Wang, F.; Tang, Y.; Zhang, Q.; Chen, M.; Shi, W.; Lin, D.; Luo, H. Theoretical analysis of high electromechanical coupling surface acoustic wave propagating on lead-free Na<sub>0.5</sub>Bi<sub>0.5</sub>TiO<sub>3</sub>–BaTiO<sub>3</sub> single crystal. *Scripta Mater* **2020**, *178*, 372–375. [[CrossRef](#)]
31. Li, X.; Bao, J.; Qiu, L.; Matsuo, N.; Omori, T.; Hashimoto, K.Y. 3D FEM simulation of SAW resonators using hierarchical cascading technique and general purpose graphic processing unit. *Jpn. J. Appl. Phys.* **2019**, *58*, SGGC05. [[CrossRef](#)]
32. Dühring, M.B.; Laude, V.; Khelif, A. Energy storage and dispersion of surface acoustic waves trapped in a periodic array of mechanical resonators. *J. Appl. Phys.* **2009**, *105*, 093504. [[CrossRef](#)]
33. Graczykowski, B.; Alzina, F.; Gomis-Bresco, J.; Sotomayor Torres, C.M. Finite element analysis of true and pseudo surface acoustic waves in one-dimensional phononic crystals. *J. Appl. Phys.* **2015**, *119*, 025308. [[CrossRef](#)]
34. Maouhoub, S.; Aoura, Y.; Mir, A. FEM simulation of AlN thin layers on diamond substrates for high frequency SAW devices. *Diam. Relat. Mater.* **2016**, *62*, 7–13. [[CrossRef](#)]
35. Maouhoub, S.; Aoura, Y.; Mir, A.J.M.E. FEM simulation of rayleigh waves for SAW devices based on ZnO/AlN/Si. *Microelectron. Eng.* **2015**, *136*, 22–25. [[CrossRef](#)]
36. Hartmann, C.S.; Jen, S.; Martin, T.A. A compact high-performance EWC/SPUDT SAW Channelizer. In Proceedings of the IEEE Ultrasonics Symposium, Prague, Czech Republic, 21–25 July 2013; pp. 1395–1398. [[CrossRef](#)]
37. Hashimoto, K.Y. *Surface Acoustic Wave Devices in Telecommunications Modeling and Simulation*; Springer: New York, NY, USA, 2000; pp. 191–235.
38. Biryukov, S.V.; Martin, G.; Schmidt, H.; Wall, B. SPUDT cell with one-wavelength period and quarter-wavelength electrodes. In Proceedings of the IEEE Ultrasonics Symposium, Orlando, FL, USA, 18–21 October 2011; pp. 1337–1340. [[CrossRef](#)]
39. Ito, H.; Hasegawa, K.; Matsuki, T.; Kusumoto, S. Lift-off photoresists for advanced IC packaging metal patterning. In Proceedings of the 16th International Conference on Electronic Packaging Technology (ICEPT), Changsha, China, 11–14 August 2015; pp. 1352–1356. [[CrossRef](#)]
40. Berkoh, D.; Kulkarni, S. Challenges in Lift-Off Process Using CAMP Negative Photoresist in III–V IC Fabrication. *IEEE Trans. Semicond. Manuf.* **2019**, *32*, 513–517. [[CrossRef](#)]
41. Kanouni, F.; Amara, S.; Assali, A.; Arab, F.; Qin, Z. A P-matrix-based model for the frequency analysis of IDT/AlScN/Sapphire SAW-delay Line. *Sensor Actuat. A Phys.* **2020**, *307*, 111980. [[CrossRef](#)]
42. Abbott, B.P. Coupling-of-Modes Model for Saw Transducers with Arbitrary Reflectivity Weighting. Ph.D. Thesis, University of Central Florida, Orlando, FL, USA, 1989.
43. Chen, Y.Y.; Wu, T.T.; Chou, T.T. Analysis of the frequency response of a dispersive IDT/ZnO/Sapphire SAW filter using effective permittivity and the coupling of modes model. *J. Phys. D Appl. Phys.* **2003**, *37*, 120–127. [[CrossRef](#)]